Materials Advances

Accepted Manuscript

This article can be cited before page numbers have been issued, to do this please use: A. Enferadikerenkan, S. Kaliaguine, F. Fontaine and A. Darvish, *Mater. Adv.*, 2026, DOI: 10.1039/D6MA00580B.

ROYAL SOCIETY OF CHEMISTRY

rsc.li/materials-advances

View Article Online
DOI: 10.1039/D6MA00580B

ARTICLE

Heterogenized Phosphonium Salt Catalysts for Cyclic Carbonate Production from CO_2 and Epoxides

Received 00th January 20xx,
Accepted 00th January 20xx

DOI: 10.1039/x0xx00000x

Afshin Enferadikerenkan [a], Ali Darvish [b], Serge Kaliaguine*[a], and Frédéric-Georges Fontaine*[b]

Building on our recent homogeneous catalyst system, this work explores heterogenization by formation of covalent organic frameworks to enhance durability. Four pyridyl-functionalized porous ionic polymers (**PPIPs**) bearing phosphonium salts were synthesized and systematically evaluated for the solvent-free cycloaddition of CO_2 to epoxides. The *para*-substituted catalyst (**4-PPIP**) exhibited superior activity compared to ortho- and meta-isomers, achieving 90% yield of styrene carbonate over 24 h at 100 °C and 0.1 MPa CO_2. Protonation of the pyridyl nitrogen (**4-PPIP-H$^+$**) enhanced catalytic efficiency 2.3-fold under catalyst-limited conditions while maintaining stability throughout extended operation. Optimization studies revealed that polymerization of the functionalized monomer outperforms the post-functionalization of the polymer. Under optimized conditions (120 °C, 6 h and 0.1 MPa CO_2), **4-PPIP-H$^+$** achieved near-quantitative conversion for styrene oxide (98%) and for a range of terminal epoxides including bio-based terpenes. Catalyst recyclability was confirmed over 4 cycles. These findings establish structure-activity relationships for heterogeneous phosphonium catalysts and provide design principles for metal-free CO_2 utilization systems.

Introduction

The escalating atmospheric CO_2 levels and its detrimental environmental impacts have spurred global efforts to develop carbon capture and utilization technologies.[1] These processes not only mitigate CO_2 emissions but also convert this greenhouse gas into industrially relevant chemicals, aligning with circular economy principles.[2-4] Among the various chemicals that have been synthesized directly from carbon dioxide, cyclic carbonates stand out as promising chemicals since they are highly valuable and its synthesis from epoxides and CO_2 is 100% atom economical.[5-7] This process can replace the typical synthesis of cyclic carbonates using toxic reagents like phosgene[8] and is already exploited industrially, notably in the production of high-purity ethylene carbonate (EC) and dimethyl carbonate by Asahi Kasei Corporation since 2002 in Japan,[9] and propylene carbonate and EC by Huntsman Corporation since the early 2000s in the USA.[10] Cyclic carbonates serve as versatile precursors for polycarbonates, electrolytes in lithium-ion batteries, polar solvents, and fuel additives.[11, 12] However, efficient catalytic systems are required to overcome the inertness of CO_2.[13-15]

Metal-based catalysts, such as Al-porphyrins,[16] Zn-salen complexes,[17] and metal-organic frameworks (MOFs),[18] have demonstrated high activity in CO_2 cycloaddition due to their Lewis acidic metal centers, which activate epoxides via coordination.[19-21] For example, zirconium and hafnium -based UiO-66 offer exceptional stability and tunability under solvent-free conditions,[22] while guanidinium-functionalized Zr-MOFs introduce Brønsted basic sites for enhanced performance.[23] However, many efficient metallic systems rely on expensive rare earths or toxic metals, for instance, polyoxovanadate–resorcinarene PMOFs (Co/V),[24] luminescent Yb/Er/Tm/Lu mesocates,[25] Er/Yb coordination polymers,[26] and benchmark Cr-salen complexes,[27] limiting scalability due to cost and toxicity concerns. In contrast, non-metal catalysts, particularly ionic liquids (ILs) and porous organic polymers (POPs), offer cost-effective alternatives with comparable or superior tunability.[17, 28, 29] Halide-based ILs, such as quaternary ammonium or phosphonium salts, activate epoxides via nucleophilic anions (e.g., Cl^-) while avoiding metal contamination.[30, 31] However, many conventional ILs necessitate the use of co-catalysts or solvents to achieve sufficient activity, which complicates product isolation and escalates operational expenses.[32] Additionally, many ILs exhibit limited thermal stability, with decomposition pathways leading to inactive byproducts like phosphine oxides.[33, 34] Recent advances in covalent organic frameworks (COFs) have addressed some limitations by integrating nucleophilic halides and Lewis acidic sites into porous matrices.[35, 36] However, achieving a balance between high surface area, active site density, and structural stability remains challenging.[37, 38]

Phosphonium salt-functionalized heterogeneous catalysts have emerged as robust alternatives, combining the nucleophilicity of halide anions with the structural integrity of porous supports.[39, 40] Early studies highlighted the role of quaternary phosphonium cations in stabilizing halides enabling epoxide ring-opening at atmospheric pressure.[41, 42] Recent innovations,

[a] Chemical Engineering Department, Université Laval, G1V 0A6, Québec City, Canada
[b] Chemistry Department, Université Laval, G1V 0A6, Québec City, Canada
* serge.kaliaguine@gch.ulaval.ca
* frederic.fontaine@chm.ulaval.ca

DOI: 10.1039/D6MA00580B

such as AlPor-QP@POP, employ a "two-in-one" design to co-polymerize aluminum porphyrin and phosphonium monomers, yielding bifunctional catalysts with high surface areas (281 $m^2 g^{-1}$) and recyclability (>10 cycles).[16] Similarly, TSP-AlCl-PhospBr, a copolymer integrating Al-porphyrin and vinyl-phosphonium units, achieves turnover numbers (TONs) of 14,500 at 80 °C, outperforming homogeneous counterparts.[42] Notable recent phosphonium/boron systems from Kilic and coworkers demonstrate high ECH carbonate yields in short times: phosphonium-boron catalysts (95%, 1.6 MPa, 100 °C + DMAP)[43]; phosphonium-salen boron (96% under similar conditions)[44]; B-ZnO nanoplates (99%, ambient pressure + PPNCl)[45]; and ZnO/BD-g-C_3N_4 (98%, ambient + PPNCl)[46]. These highlight halide/Lewis acid synergy, motivating our metal-free PPIPs with tunable pyridyl sites for atmospheric pressure operation.

Despite these advances, key challenges persist. The symmetry and reactivity of monomers critically influence pore uniformity and active site distribution.[47] For instance, irregular stacking in phosphonium-based porous ionic polymers (PIP) often reduces CO_2 adsorption capacity (<1.1 mmol g^{-1}) and mass transfer efficiency.[16] Moreover, the chemical stability of phosphonium salts under prolonged reaction conditions remains understudied. Zhong et al. revealed that asymmetric flexible alkyl chains in phosphonium ILs mitigate decomposition by shielding the cation center, reducing phosphine oxide formation while maintaining >99% carbonate yields.[33] Such insights underscore the need for tailored cationic architecture to enhance both activity and longevity.

In this study, we report the synthesis and catalytic evaluation of a new series of pyridyl-functionalized triphenylphosphonium-based porous ionic polymers (PPIPs), a class of covalent organic frameworks for the solvent-free cycloaddition of CO_2 to epoxides. Building upon our previous findings with homogeneous pyridylphosphonium catalysts,[48] this work aims at (i) exploring the effect of pyridine substitution patterns (*ortho*-, *meta*-, and *para*-) on catalytic activity in a heterogeneous environment, (ii) assessing the influence of Brønsted acidity by protonating the most active catalyst, and (iii) comparing different catalyst architectures based on the timing of phosphonium grafting, before versus after polymerization. The study seeks to provide a comprehensive structure–activity relationship that bridges catalyst design, synthetic strategy, and performance in CO_2 conversion, offering valuable insight into the development of efficient, stable, and recyclable metal-free catalysts for green chemistry applications.

Experimental

Materials

All glassware was dried overnight at 100 °C and purged with vacuum/nitrogen cycles. 3-Pyridinemethanol, magnesium powder, dibromoethane, thionyl chloride, and epoxides were obtained from Sigma-Aldrich (except for limonene dioxide, which was purchased from Ambeed), while 2- and 4-pyridinemethanol and 4-bromostyrene were purchased from Oakwood. THF was dried using a solvent purification system (SPS), and $CDCl_3$ was dried over molecular sieves. Additional materials information is provided in Supporting Information (SI).

Characterization methods

NMR spectra were recorded on a Varian Inova DD2 spectrometer at 500 MHz (^{1}H), 125.76 MHz (^{13}C), 202.456 MHz (^{31}P). ^{1}H, ^{13}C, ^{31}P NMR spectra were referenced to Me_4Si (^{1}H, ^{13}C), 85 % H_3PO_4 (^{31}P). Multiplicities are reported as singlet (s), doublet (d), triplet (t), quadruplet (q), quintuplet (p), and multiplet (m). Chemical shifts are reported in ppm. Coupling constants (J) are reported in Hz. NMR spectra were processed using MestReNova 9.0.

The synthesized catalysts were characterized using Fourier-transform infrared (FT-IR) spectroscopy. Static FT-IR measurements were performed on an ABB MB-3000 spectrometer equipped with a deuterated triglycine sulfate (DTGS) detector and a horizontal attenuated total reflectance (HATR) accessory with a ZnSe crystal. Spectra were recorded in the range of 4000–400 cm^{-1} at a resolution of 4 cm^{-1}, averaging 64 scans per sample to ensure signal-to-noise optimization. Background scans were collected under identical conditions prior to sample analysis and subtracted automatically using the Horizon MB™ software.

Thermogravimetric analysis (TGA) was conducted utilizing a Netzsch STA 449 C thermal analyzer, with measurements performed at a heating progression of 5 °C per minute while maintaining a consistent air flow of 20 milliliters per minute. The CHN elemental analysis was conducted using a Thermo Scientific™ FLASH 2000 CHNS/O analyzer. Nitrogen adsorption–desorption isotherms were recorded using a Micromeritics Autosorb-iQ1 surface area and porosity analyzer. Prior to analysis, the phosphonium-functionalized polymeric catalysts were degassed under vacuum at 150 °C for 12 hours to remove adsorbed moisture and gases. The specific surface area was calculated using the Brunauer–Emmett–Teller (BET) method in the relative pressure range of P/P_0 = 0.05–0.20. The total pore volume was determined from the volume of nitrogen adsorbed at P/P_0 = 0.95. CO_2 adsorption isotherms were measured using a Micromeritics Tristar™ II 3020 instrument at 273 K and 298 K, employing an ice-water and ambient temperature bath, respectively.

Synthesis

Synthesis of tris(4-vinylphenyl)phosphine.[49] Magnesium powder (7.29 g, 300 mmol) was added to a flame-dried round-bottom flask under N_2. Anhydrous THF (200 mL) was added, along with 1,2-dibromoethane (0.5 mL) to initiate the radical activation of Mg. Subsequently, the reaction mixture was cooled to 0 °C using ice. A solution of 4-bromostyrene (24.7 g, 135 mmol) in 10 mL THF was slowly added; then, the mixture was left stirring for 2 hours at 0 °C. A solution of PCl_3 (4.63 g, 33.8 mmol) in 10 mL THF was added to the mixture over 1 hour at 0 °C and then warmed up to room temperature and stirred for 8 hours. Then, the reaction mixture was quenched with saturated NH_4Cl(aq) (20 mL); the solution color changed to white. The organic phase was extracted using diethyl ether (30

View Article Online
DOI: 10.1039/D6MA00580B

mL × 3) and dried over $MgSO_4$. After filtering and concentrating under vacuum, yellowish crude oil was obtained. By using silica gel chromatography (5% EtOAc/Petroleum ether), a pure white solid was obtained (41 %, 4.71 g) (**Scheme 1**). The collected

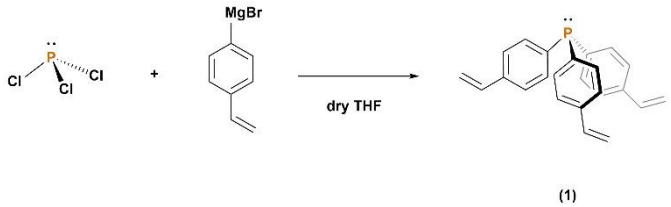

(1)

NMR spectrum matches that of literature.[29, 41, 49]

Tris(4-vinylphenyl)phosphine (**1**): ^{1}H NMR (500 MHz, $CDCl_3$) δ (ppm): 7.40 (dd, *J* = 8.0, 1.5 Hz, 6H), 7.30 (t, *J* = 7.7 Hz, 6H), 6.72 (dd, *J* = 17.6, 10.9 Hz, 3H), 5.80 (d, *J* = 17.6 Hz, 3H), 5.30 (d, *J* = 10.9 Hz, 3H). ^{13}C{^{1}H} NMR (126 MHz, $CDCl_3$) δ 138.0 (s), 136.6 (d, *J* = 10.4 Hz), 136.4 (s) , 133.8 (d, $^1J_{C\text{-}P}$ =19.6 Hz), 126.4(d, *J* = 7.1 Hz), 114.8 (s). ^{31}P{^{1}H} NMR (202 MHz, $CDCl_3$) δ -6.8 ppm.

Scheme 1. Synthesis of tris(4-vinylphenyl)phosphine (**1**) by Grignard reaction

Synthesis of (pyridinylmethyl)tris(4-vinylphenyl)phosphonium chloride (2-, 3-, and 4- position). The chlorinated pyridinylmethyl derivatives (2-chloromethylpyridine (**2**), 3-chloromethylpyridine (**3**), and 4-chloromethylpyridine (**4**)) were prepared following the procedure described in our previous work.[48] Corresponding (chloromethyl)pyridine (0.35 g, 2.76 mmol) and tris-(4-vinylphenyl)-phosphine (**1**) (0.78 g, 2.30 mmol) were dissolved in acetone (5 mL) and stirred for 48 hours at 65 °C under N_2 atmosphere. Following the reaction, the mixture was cooled to room temperature before being filtered, washed with diethyl ether, and dried under vacuum to obtain (pyridine-2-ylmethyl)tris(4-vinylphenyl)phosphonium chloride (**2**) as a rose solid, (pyridine-3-ylmethyl)tris(4-vinylphenyl)phosphonium chloride (**3**) as a bright rose solid, and (pyridine-4-ylmethyl)tris(4-vinylphenyl)phosphonium chloride (**4**) as an orange solid (**Scheme 2**).

(Pyridine-2-ylmethyl)tris(4-vinylphenyl)phosphonium chloride (**2**) (84%): ^{1}H NMR (500 MHz, $CDCl_3$) δ (ppm): 8.24 (ddd, *J* = 5.0, 2.0, 0.9 Hz, 1H), 8.02 (d, *J* = 7.9 Hz, 1H), 7.84 – 7.76 (m, 6H), 7.63 – 7.55 (m, 7H), 7.12 (t, *J* = 6.3 Hz, 1H), 6.73 (dd, *J* = 17.6, 10.9 Hz, 3H), 5.92 (d, *J* = 17.6 Hz, 3H), 5.77 (d, *J* = 14.5 Hz, 2H), 5.49 (d, *J* = 10.9 Hz, 3H). ^{13}C{^{1}H} NMR (126 MHz, $CDCl_3$, ppm), δ: 148.1 (s), 143.6 (d, *J* = 3.1 Hz), 135.1 (d, *J* = 1.9 Hz), 134.5 (d, *J* = 10.5 Hz), 127.4 (d, *J* = 13.4 Hz), 118.9 (s), 117.4 (d, $^1J_{C\text{-}P}$ = 89.6 Hz), 32.2 (d, $^2J_{C\text{-}P}$ = 51.6 Hz). ^{31}P{1H} NMR (202 MHz, $CDCl_3$) δ 23.1 ppm. HRMS (ESI$^+$) m/z: Calcd for $C_{30}H_{27}NP^+$ [M]$^+$ 432.1876; found 432.1812.

(pyridine-3-ylmethyl)tris(4-vinylphenyl)phosphonium chloride (**3**) (76%): ^{1}H NMR (500 MHz, $CDCl_3$) δ (ppm): 8.43 (dd, *J* = 4.9, 2.5 Hz, 1H), 8.13 (s, 1H), 8.06 (d, *J* = 7.9 Hz, 1H), 7.81 – 7.73 (m, 7H), 7.62 (dd, *J* = 8.5, 3.1 Hz, 7H), 7.15 (dd, *J* = 7.9, 4.9 Hz, 1H), 6.75 (dd, *J* = 17.6, 10.9 Hz, 3H), 5.95 (d, *J* = 17.6 Hz, 3H), 5.77 (d, *J* = 14.8 Hz, 2H), 5.53 (d, *J* = 10.9 Hz, 3H). ^{13}C{^{1}H} NMR (126 MHz, $CDCl_3$, ppm), δ: 150.5 (s), 144.1 (d, *J* = 2.9 Hz), 134.9 (d, *J* = 1.9 Hz), 134.7 (d, *J* = 10.4 Hz), 127.8 (d, *J* = 13.3 Hz), 124.0 (s), 119.4 (s), 115.9 (d, $^1J_{C\text{-}P}$ = 88.2 Hz), 28.0 (d, $^2J_{C\text{-}P}$ = 49.5 Hz). ^{31}P NMR{^{1}H} (202 MHz, $CDCl_3$) δ 23.2 ppm. HRMS (ESI$^+$) m/z: Calcd for $C_{30}H_{27}NP^+$ [M]$^+$ 432.1876; found 432.1845.

(pyridine-4-ylmethyl)tris(4-vinylphenyl)phosphonium chloride (**4**) (88%): ^{1}H NMR (500 MHz, $CDCl_3$) δ (ppm): 8.24 (ddd, *J* = 5.0, 1.9, 0.9 Hz, 1H), 8.02 (d, *J* = 7.9 Hz, 1H), 7.84 – 7.76 (m, 6H), 7.63 – 7.55 (m, 7H), 7.12 (t, *J* = 6.3 Hz, 1H), 6.73 (dd, *J* = 17.6, 10.9 Hz, 3H), 5.92 (d, *J* = 17.6 Hz, 3H), 5.77 (d, *J* = 14.5 Hz, 2H), 5.49 (d, *J* = 10.9 Hz, 3H). ^{13}C{^{1}H} NMR (126 MHz, $CDCl_3$, ppm), δ: 148.4 (s), 144.1 (d, *J* = 3.2 Hz), 134.9 (d, *J* = 1.9 Hz), 134.7 (d, *J* = 10.5 Hz), 127.7 (d, *J* = 13.3 Hz), 127.2 (s), 119.4 (s), 115.8 (d, $^1J_{C\text{-}P}$ = 88.7 Hz), 30.0 (d, $^2J_{C\text{-}P}$ = 47.8 Hz). ^{31}P{^{1}H} NMR (202 MHz, $CDCl_3$) δ 23.4 ppm. HRMS (ESI$^+$) m/z: Calcd for $C_{30}H_{27}NP^+$ [M]$^+$ 432.1876; found 432.1803.

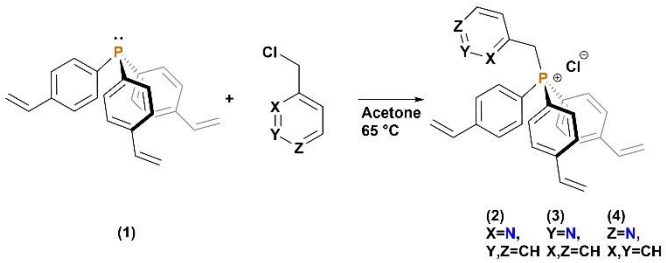

Scheme 2. Synthesis of (pyridinylmethyl)tris(4-vinylphenyl)phosphonium chloride (2-, 3-, and 4- positions).

Synthesis of 2-, 3- and 4-PPIP and 4-PPIP-Alt (Alternative polymerization). The synthesized monomers (**2**, **3**, and **4**) were each dissolved (0.29 g) in 4 mL of DMF along with 7 mg of azobisisobutyronitrile (AIBN) as the radical initiator. The mixtures were stirred at room temperature until fully homogeneous, then transferred to an autoclave and heated at 100 °C for 24 hours to effect polymerization. After cooling, the resulting polymers (**2-, 3-,** and **4-PPIP**) were isolated by repeated washing with diethyl ether and methanol, combined with centrifugation, to remove unreacted monomers and impurities. The purified polymers were then dried under vacuum before further characterization and use.

To explore an alternative synthetic route for **4-PPIP**, a reverse order method was employed. First, tris(4-vinylphenyl)phosphine (**1**) was polymerized under the same conditions (100 °C, 24 hours, AIBN initiation) to yield **PIP**. Subsequently, the resulting polymer was reacted with 4-(chloromethyl)pyridine (0.35 g, 2.76 mmol) in acetone (5 mL) at 65 °C for 48 hours under nitrogen atmosphere. After reaction completion, the mixture was cooled, filtered, washed with diethyl ether, and dried under vacuum to yield the functionalized polymer **4-PPIP-Alt** (**Scheme 3**) as a slightly brighter solid compared to **4-PPIP** (89% yield).

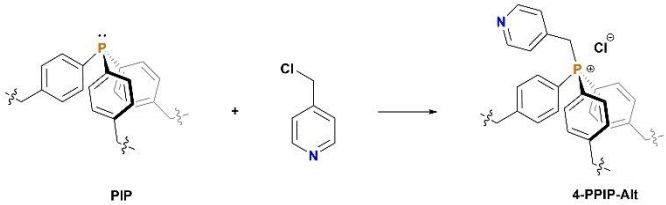

Scheme 3. Synthesis of **4-PPIP**-Alt from **PIP**

View Article Online DOI: 10.1039/D6MA00560B

Synthesis of protonated catalyst 4-PPIP-H⁺. The protonation procedure for catalyst **4-PPIP-H⁺** was adapted from the method reported in our previous work with the key modification of using methanol as the solvent instead of chloroform.[48] Briefly, the catalyst was suspended in methanol, and gaseous HCl was generated on site by reacting sodium chloride with concentrated sulfuric acid. The HCl gas was bubbled through the catalyst solution while stirring overnight. The resulting protonated catalyst was then filtered, washed three times with diethyl ether to remove impurities, and dried under vacuum.

CO_2 cycloaddition of epoxides

The cycloaddition reactions were conducted by loading the selected epoxide (2.5-5 mmol) and the catalyst into a 20 mL batch glass reactor equipped with a magnetic stirring bar. The reactor was charged with CO_2 at atmospheric pressure, and the mixture was stirred at a constant temperature ranging from 25 °C to 120 °C for the required duration. After the reaction, the reactor was cooled to room temperature. Post-reaction, the mixture was centrifuged to recover the catalyst, and the supernatant was analyzed by ^{1}H NMR spectroscopy with mesitylene being used as a standard compound. Product selectivity was determined from the NMR integrals. For most substrates, no major side products were detected, except glycidol, which gave glycerol carbonate and glycerol as the main product and by-product, respectively.

Results and discussion

Materials Characterization

Our previous report demonstrated that the presence of the pyridinium moiety on the phosphonium helped improve catalytic activity in the cycloaddition reaction between epoxides and CO_2 to generate cyclic carbonates.[48] The protonation of the catalysts did improve the rate of catalytic transformations at the cost of lower stability. Since the degradation pathway was bimolecular, it was hypothesized that a heterogeneous analogue might improve catalytic stability. The synthesis of the covalent organic frameworks was achieved through AIBN-initiated free-radical polymerization of vinyl-functionalized phosphonium salt monomers, affording the corresponding cross-linked polymer networks (**2-**, **3-**, and **4-PPIP**).

All synthesized **PPIP** catalysts were systematically characterized to confirm their structure and assess key physicochemical properties relevant to catalysis. Elemental CHN analysis (**Table 1**) allowed verifying the incorporation of the pyridylphosphonium functionality, with nitrogen contents ranging from 1.55% for **4-PPIP-Alt** to 3.36% for **3-PPIP**, **4-PPIP** and **4-PPIP-H⁺** each displayed high nitrogen levels (3.16% and 3.04%), confirming the retention of active sites after protonation. Carbon and hydrogen values were consistent throughout, indicating successful polymer backbone formation.Table 1. Elemental and textural properties of all PPIP catalysts. Nitrogen, carbon, and hydrogen contents (CHN), BET surface area, pore volume, and average pore size are shown.

Catalyst	N (%)	C (%)	H (%)	BET S.A. (m^2/g)	Pore Volume (cm^3/g)	Pore Radius (Å)
2-PPIP	2.74	67.23	4.60	287	0.101	17
3-PPIP	3.36	66.47	4.64	260	2.007	19
4-PPIP	3.16	66.77	4.73	74.9	0.522	15
4-PPIP-Alt	1.55	67.53	4.90	357.2	0.359	22
4-PPIP-H⁺	3.04	66.72	5.02	43	0.194	33

Textural properties were probed by nitrogen physisorption, revealing systematic trends across the **PPIP** catalyst family (**Table 1**). **2-PPIP** exhibited a moderate surface area (287 m^2/g), while **3-PPIP** showed exceptionally high pore volume (2.007 cm^3/g). **4-PPIP** displayed balanced porosity (74.9 m^2/g, 0.522 cm^3/g, 15.3 Å), while **4-PPIP-Alt** displayed the highest surface area (357.2 m^2/g, 0.359 cm^3/g, 22 Å), and protonated **4-PPIPH⁺** enlarged pores (33 Å) with reduced capacity (43 m^2/g, 0.194 cm^3/g). N_2 adsorption–desorption isotherms (**Figure 1**) from duplicate runs per catalyst showed Type *IV* profiles with low-P hysteresis ($P/P_0 \approx 0.4$), characteristic of N_2-induced swelling in polymers, most pronounced in **4-PPIP-Alt**. Replicates were reproducible (e.g., **2-PPIP**: 237–295 m^2/g; **3-PPIP**: 90–260 m^2/g), and literature confirms irreversible pore opening in porous organic networks upon nitrogen physisorption.[50, 51]

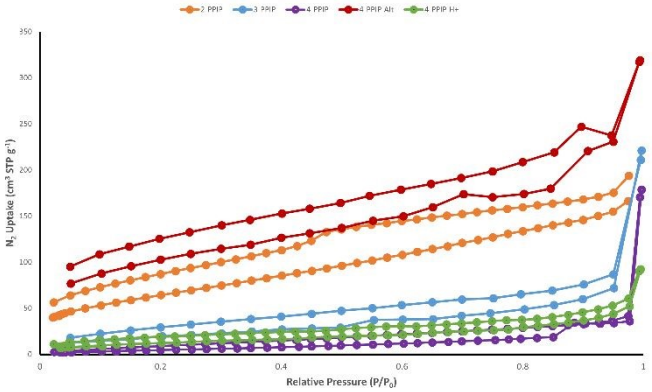

Figure 1. Nitrogen adsorption isotherms of all catalysts at 77 K, highlighting differences in porosity and surface area.

FT-IR spectroscopy was used to establish the presence of characteristic aromatic backbone with vibrations corresponding to C=N stretches (1560–1650 cm^{-1}), and, in the protonated material, a diagnostic broad H–N band (3200–3600 cm^{-1}) and subtle shifts in the fingerprint region. These spectroscopic variations confirm both functional group installation and subsequent Brønsted acidification (**Figure 2**).

View Article Online
DOI: 10.1039/D6MA00580B

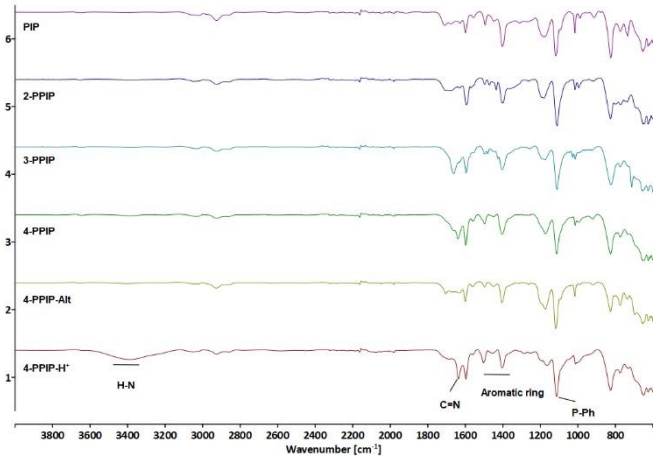

Figure 2. FT-IR spectra of PIP and pyridyl-functionalized phosphonium salts, showing the N–H band (~3300 cm^{-1}), C=N band (~1640–1660 cm^{-1}), and P-phenyl band (~1110 cm^{-1}).

Solid-state ^{13}C and ^{31}P NMR spectra further corroborated polymer structure. All catalysts gave intense resonances for aromatic and pyridyl carbons, and a narrow ^{31}P signal centered near 22–23 ppm ascribed to the quaternized phosphonium group. Upon protonation, a noticeable downfield shift in ^{31}P was observed, supporting electronic modification of the pyridine ring (Figure S19-S23).

Thermogravimetric analysis allowed demonstrating the outstanding stability for both **4-PPIP** and **4-PPIP-H$^+$**, with only minor (<5%) mass loss below 200 °C attributed to residual water and solvent, and principal decomposition temperatures above 450 °C. This confirms suitability for elevated-temperature catalysis (Figure S24, S25).

Together, these results confirm the successful synthesis and robust architecture of the polymeric pyridylphosphonium catalysts, highlighting the impact of functionalization sequence and protonation on material properties. Complete analytical data, individual spectra and isotherms, and further details are reported in the Supporting Information.

Catalytic experiments

The catalytic performance of the heterogeneous pyridyl-functionalized triphenylphosphonium polymers was investigated in the cycloaddition of CO_2 to styrene oxide under solvent-free conditions (**Table 2**). SO was selected as a benchmark substrate for optimization and catalyst comparison because it is a more demanding epoxide, consistent with our aim of testing the catalyst on less activated and sterically challenging substrates. The tests were carried out at 100 °C and 0.1 MPa CO_2 pressure for 24 hours using 25 mg of catalyst. A control reaction without catalyst resulted in no detectable product formation, confirming the necessity of catalytic activation under these mild conditions (Entry 1). The **PIP** catalyst (Entry 2, 6% yield) performed identically to PPh_3 (5.3% yield) from our previous homogeneous catalytic system,[48] confirming the phosphonium core as the active motif and that the neutral phosphine was inactive for catalysis.

The *para*-substituted catalyst (**4-PPIP**) demonstrated the highest activity, achieving a 90% yield of the styrene carbonate, whereas **3-PPIP** and **2-PPIP** gave 73% and 43%, respectively (Entry 3-5). This trend supports the hypothesis that positional effects of the pyridyl ring influence catalytic efficiency, likely due to differences in electronic distribution and in cooperativity between the pyridine and the halide in the activation process. These findings are consistent with our previous study on pyridylmethyl-functionalized phosphonium salts acting as homogeneous catalysts (2-6% loading, 6 mol% optimized), where *para*-substitution similarly led to superior activity.[48] Notably, **4-PPIP** (Entry 5) and **4-PPIP-H$^+$** (Entry 6) at ~2.2 mol% catalyst loading matches the excellent yield of homogeneous $[(4\text{-}PyCH_2)PPh_3]Cl$ (91% at 2 mol%, 80 °C).

Our previous work on homogeneous pyridylmethyl-functionalized triphenylphosphonium catalysts demonstrated that protonation of the pyridyl nitrogen can significantly accelerate the cycloaddition of CO_2 to epoxides.[48] This enhancement came however, at the cost of reduced catalyst stability, with accelerated degradation observed over extended reaction times. Motivated by these findings, investigation of whether similar protonation effects could be leveraged in the heterogeneous system while potentially mitigating the stability issues through the structural integrity of the COF, was undertaken.

Table 2. Cycloaddition of CO_2 to styrene oxide[a].

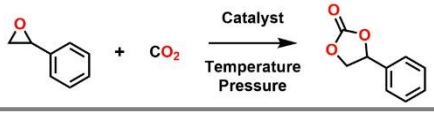

Entry	Catalyst	Catalyst Loading (mg)	mol% N[b]	Yield (%)[c]
1	None	0	0	n.r. [d]
2	PIP	25	2.9[e]	6
3	2-PPIP	25	2.0	43
4	3-PPIP	25	2.4	73
5	4-PPIP	25	2.3	90
6	4-PPIP-H$^+$	25	2.2	93
7	4-PPIP-Alt	25	1.1	12
8	4-PPIP	15	1.4	36
9	4-PPIP-H$^+$	15	1.3	81

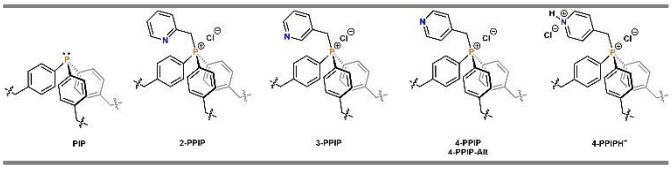

[a] Reaction conditions: styrene oxide (2.5 mmol), CO_2 pressure (0.1 MPa), temperature (100 °C), co-catalyst and solvent-free, 24 hours.
[b] From CHN analysis (wt% N/14.007)
[c] The yield was defined as a molar ratio of carbonate to initial epoxide.
[d] n.r. = no reaction
[e] From monomer M_W ($C_{24}H_{21}P$, 340.41 g/mol)

Catalyst **4-PPIP**, identified here as the most active heterogeneous catalyst, allowed achieving a 90% yield of cyclic carbonate from styrene oxide after 24 hours at 100 °C under atmospheric CO_2 pressure using 25 mg catalyst loading (**Table**

2, Entry 5). Initial comparison at 25 mg catalyst loading revealed only marginal differences between the two catalysts, **4-PPIP** achieved 90% yield, while **4-PPIP-H$^+$** gave 93% yield (**Table 2**, Entries 5 and 6).

To better illustrate the role of protonation, the catalyst loading was reduced to 15 mg, creating more challenging conditions that would amplify any differences in intrinsic activity. Under these conditions, the effect of protonation became remarkably pronounced. After 24 hours, **4-PPIP** delivered only 36% yield (**Table 2**, Entry 8), whereas **4-PPIP-H$^+$** achieved 81% yield (**Table 2**, Entries 8 and 9). This dramatic performance gap highlights the significant role of Brønsted acidity in activating the catalytic cycle.

Notably, unlike the homogeneous system where protonation led to rapid catalyst degradation via phosphine oxide formation (^{31}P NMR δ ≈ 30 ppm),[48] FT-IR analysis (Figure S26) confirmed the heterogeneous **4-PPIP-H$^+$** remained completely stable after 24 h cycloaddition without signs of degradation. This outcome underscores a key advantage of heterogenization; the covalent organic framework appears to stabilize the protonated catalyst, preserving both the activity benefits conferred by Brønsted acidity and the structural integrity of the active sites over extended operation.

Two complementary synthetic routes were explored to assess how monomer sequencing influences catalyst composition, textural properties, and CO_2 cycloaddition performance. In direct monomer polymerization, 4-chloromethylpyridine reacted with tris(4-vinylphenyl)phosphine to form the vinyl-phosphonium monomer, which was copolymerized with divinylbenzene (AIBN, toluene, 70 °C). Elemental analysis of **4-PPIP** confirmed high pyridyl incorporation (3.16 wt% N). BET analysis showed moderate surface area (74.9 m^2/g), high pore volume (0.522 cm^3/g), and narrow mesopores (15.3 Å). Furthermore, pore distribution confirms most pores in the 15–35 Å range, ideal for substrate access.

By contrast, the post-functionalization route first copolymerized tris(4-vinylphenyl)phosphine with divinylbenzene, then grafted 4-chloromethylpyridine to give **4-PPIP-Alt**. The latter polymer has a lower N-loading (1.55 wt% N), likely due to diffusion limits reducing the number of successful grafting. BET revealed higher surface area (357.2 m^2/g) and larger pores (21.6 Å), but reduced pore volume (0.359 cm^3/g). The DH distribution shows this high surface area arises from additional mesopores (20–50 Å) created during grafting, while smaller pores (<20 Å) were blocked, explaining the lower pore volume. As shown in **Figure 3**, the two synthetic routes led to markedly different catalyst compositions and textural properties, which were reflected in their catalytic performance. Under standard reaction conditions (styrene oxide, 2.5 mmol; 100 °C; 0.1 MPa CO_2; 25 mg catalyst; 24 h), **4-PPIP** delivered 90% styrene carbonate yield, while **4-PPIP-Alt** yielded only 12% (**Table 2**, Entry 7). This stark contrast reveals that active site density and pore accessibility, not surface area alone, govern performance. The post-functionalized **4-PPIP-Alt** suffers from dilute catalytic centers and compromised mesoporosity (Vp 0.359 vs 0.522 cm^3/g), despite higher BET area, limiting the diffusion of the reagents in the polymeric framework. Furthermore, the direct polymerization route embeds uniformly dispersed phosphonium sites within a balanced pore network, facilitating cooperative Lewis acidic activation by phosphonium cations and nucleophilic attack by chloride anions, which was calculated to be governing the catalytic activity of the homogeneous analogues.[48] The small interconnected pores of **4-PPIP** enable rapid diffusion of CO_2 and epoxide to active centers. In contrast, the post-functionalized network, despite its open architecture, suffers from sparse active sites and diffusion bottlenecks likely due to blocked microchannels.

Overall, these findings demonstrate that monomer functionalization prior to polymerization is essential to maximize active site incorporation and maintain an optimal balance of pore volume and surface area. Post-grafting strategies, while increasing surface area, compromise catalytic efficiency by reducing site density and obstructing diffusional mass transfer into micropores.

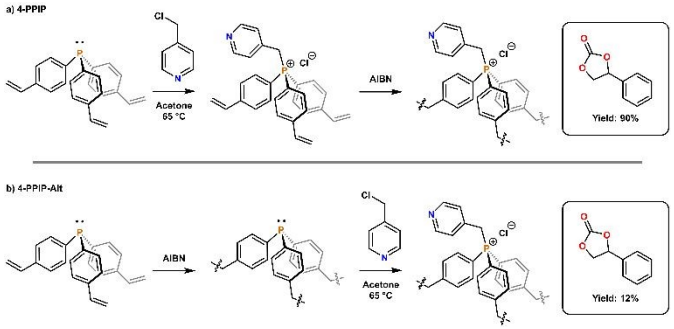

Figure 3. Comparison of the synthetic routes and *styrene* carbonate yields obtained using *a)* **4-PPIP** (*top*) and *b)* **4-PPIP-Alt** (*bottom*).

Catalyst optimization

Having identified **4-PPIP-H$^+$** as the best catalyst, systematic optimization was conducted using styrene oxide as a model substrate (2.5 mmol) and a 0.1 MPa CO_2 atmosphere. First, the effect of catalyst loading was evaluated at 100 °C for 18 h (**Figure 4a**). Loadings of 5, 10, 15, 20, and 25 mg were tested, affording yields of 25%, 61%, 76%, 84%, and 95%, respectively.

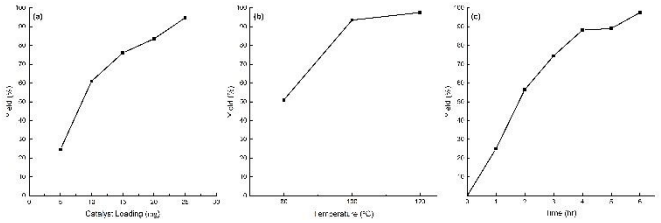

Figure 4. Optimization of reaction parameters for CO_2 cycloaddition using 4-PPIP-H$^+$ (2.5 mmol styrene oxide, 0.1 MPa CO_2). (a) Effect of catalyst loading (5–25 mg) at 100 °C for 18 h. (b) Effect of temperature (80–120 °C) at 25 mg catalyst for 12 h. (c) Effect of reaction time (1–6 h) at 25 mg catalyst and 120 °C.

Next, the influence of reaction temperature was probed at 25 mg catalyst for 12 h (**Figure 4b**). At 80 °C, the yield reached only 51%, increasing to 94% at 100 °C, and achieving 98% at 120 °C. The enhanced conversion at elevated temperature reflects faster CO_2 activation and epoxide ring opening without compromising catalyst integrity.

DOI: 10.1039/D6MA00580B

Finally, the reaction time was varied from 1 to 6 h at 25 mg catalyst and 120 °C (**Figure 4c**). Yields progressed from 25% (1 h), 57% (2 h), 75% (3 h), 88% (4 h), 89% (5 h), and plateaued at 98% after 6 h. These results confirm that 6 h is sufficient for quantitative conversion under optimized conditions.

TON and TOF were calculated from the amount of cyclic carbonate formed, the catalyst loading, and the reaction time. For SO, using 2.2 mol% N (based on CHN for 25 mg catalyst) catalyst loading and 2.5 mmol substrate, the catalyst amount gave TON values of 25.68–44.32 and TOF values of 7.39–12.84 h^{-1} depending on the product yield at 2–6 h.

Overall, the optimal conditions for CO_2 cycloaddition with **4-PPIP-H⁺** are 25 mg catalyst, 120 °C, and 6 h, providing near-quantitative yields of cyclic carbonate. These parameters were employed in all subsequent substrate scope investigations.

Catalytic activity towards different epoxides

The substrate scope of the **4-PPIP-H⁺** catalyst was evaluated using diverse terminal epoxides under optimized reaction conditions (**Table 3**). In the reaction with epichlorohydrin (Entry 1), the catalyst allowed achieving a high yield of 99%, demonstrating excellent activity toward halogenated epoxides. Epibromohydrin (Entry 2) similarly gave a high yield of 93%, consistent with the favorable effect of halogen substituents in promoting ring-opening. Glycidol (Entry 3), a hydroxyl-functionalized epoxide, was converted nearly quantitatively (79 % carbonate, 20% glycerol), indicating the catalyst's ability to tolerate polar functional groups and achieve near-complete conversion. Phenyl glycidyl ether (Entry 4) afforded a 98% yield, further illustrating the catalyst's efficiency with aromatic-substituted epoxides. These results confirm the broad applicability of **4-PPIP-H⁺** and its potential for diverse CO_2 fixation reactions in less than 6 hours.

Table 3. Cycloaddition of CO_2 to various epoxides catalyzed by **4-PPIP-H⁺** at optimal reaction conditions[a]

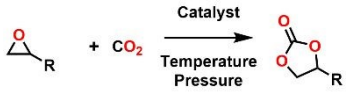

Entry	Epoxide	Carbonate	Yield (%)[b]
1		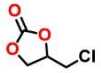	99
2		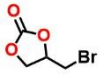	93
3		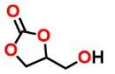	79[c]
4	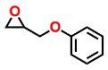	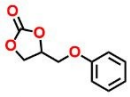	98
5		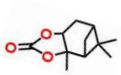	99[d]
6		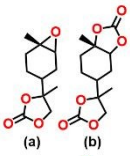	(a) 23[d] (b) 5
7			(a) 23[e] (b) 5
8	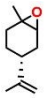	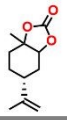	8[d]
9			28[e]

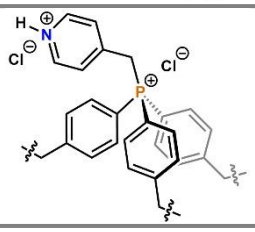

[a] Reaction conditions: catalyst **4-PPIP-H⁺** (25 mg), epoxide 2.5 mmol, CO_2 pressure (0.1 MPa), temperature (120 °C), time (6 h), co-catalyst and solvent-free. [b] The yield was determined by standard ^1H NMR (500 MHz) spectra and mesitylene is used as internal standard in $CDCl_3$. [c] The yield was determined by ^1H NMR (500 MHz) spectra in D_2O and the product revealed 79% glycerol carbonate and 20% glycerol as the main side product. [d] Time : 24 h, [e] Time: 48 h, CO_2 pressure (1 MPa).

Internal and more sterically encumbered epoxides presented greater challenges under the heterogeneous conditions. Under standard reaction conditions (120 °C, 0.1 MPa CO_2, 25 mg **4-PPIP-H⁺**, 24 h), α-pinene oxide (Entry 5) was converted almost quantitatively, giving 99% yield of the corresponding cyclic carbonate, confirming that the catalyst efficiently accommodates rigid bicyclic terpene substrates. In contrast, limonene dioxide (Entry 6) and limonene oxide (Entry 8) were much less reactive at atmospheric pressure. Even after 48 h at 0.1 MPa, LDO reached only 28% conversion (23 % monocyclic, 5% dicarbonate), while LO afforded just 8% yield, with a product mixture composed of 90% *trans* and 10% *cis* isomers.

View Article Online
DOI: 10.1039/D6MA00580B

To probe the effect of CO_2 pressure, reactions with LDO and LO were repeated at 1.0 MPa for 24 h (Entries 7, 9). Under these intensified conditions, LDO was converted in 99% yield, giving 73% monocyclic carbonate and 26% dicarbonate. In contrast, LO remained significantly less reactive, reaching 28% yield; in this case, the carbonate resonances for the cis and trans products appeared at essentially the same chemical shift in the ^{1}H NMR spectrum, making it difficult to distinguish the individual isomers, although the product is expected to be a mixture of diastereomers.

This pronounced reactivity gap between LO and α-pinene oxide underscores the key role of steric congestion around the internal epoxide in controlling reactivity. It is fully consistent with our previous homogeneous study, where DFT calculations showed that the transition state for the rate-determining step in CO_2 cycloaddition to limonene oxide is approximately 10 kcal mol^{-1} higher in free energy than for α-pinene oxide, due to the steric hindrance imposed by the pendant isopropyl group.[48]

The cycloaddition of CO_2 to terpene oxides, key to the synthesis of bio-renewable polycarbonates, confronts significant kinetic and thermodynamic hurdles due to the steric bulk, conformational rigidity of substrates, and poor CO_2 compatibility.[52, 53] Literature routinely employs pressurized CO_2 or supercritical conditions (up to 30-40 MPa)[54] to enhance reactivity, often necessitating specialized high-pressure reactors that inflate capital costs and safety concerns.[32] Homogeneous metal catalysis remains predominant, combining Lewis acidic centers (e.g., Ca, Al, Zn, Mo) with nucleophilic halide donors (e.g., TBAX, and other Bu_4N salts) and coordinating solvents (e.g., MeCN) to orchestrate epoxide activation, ring-opening, and CO_2 coupling.[55]

Table 4 positions **4-PPIP-H$^+$** within this landscape, demonstrating breakthrough ambient-pressure capability (0.1 MPa, Entry 1): 28% LDC and 8% LC (24 h) was achieved under mild conditions, outperforming [^{n}Bu$_4$N]$_2$[MoO$_4$] (9% LC despite 3 MPa; Entry 6)[56] and Zn/TBAC complexes (10–34% LC at 1–2 MPa/72 h; Entries 7–8)[57] that demand extended reaction times and additives. Even multi-component benchmarks require more demanding conditions to achieve similar activity to **4-PPIP-H$^+$**, with supported ionic liquid phase (SILP) requiring 5 MPa for 62/79% LC/LDC (Entry 3)[54], while calcium-based catalyst with PPh_3 as cocatalyst attains 80/78% LC/LDC at the same pressure after 48 h (Entry 4)[58], and Al complex/Bu_4NCl requires 66 h at 1 MPa to obtain 48/85% yields of LC/LDC (Entry 5).[59]

Table 4. Comparison of **4-PPIP-H$^+$** with literature catalysts for the synthesis of limonene carbonate from limonene oxide and limonene dicarbonate from limonene dioxide.

Ent.	Catalyst	T (°C)	P CO_2 (MPa)	Time (h)	LC[a] Yield (%)	LDC[b] Yield (%)	Ref.
1	4-PPIP-H$^+$	120	0.1	24	8	28	This work
2	4-PPIP-H$^+$	120	1.0	48	28	99	This work
3	SILP	120	5.0	20	62	79	54
4	CaI_2+ ligand	75	5.0	48	80	78	58
5	aluminum complex	80	1.0	66	48	85	59
6	[^{n}Bu$_4$N]$_2$[MoO$_4$]	120	3.0	9	9	-	56
7	[ZnMe(κ^3-Fphbp^{t}amd)]+ TBAC	70	1.0	72	10	-	57
8	[ZnMe(κ^3-phbp^{t}amd)]+ TBAC	70	2.0	72	34	-	57

[a] LC= limonene carbonate (from limonene oxide), [b] LDC= mixture of limonene mono- and dicarbonates from limonene dioxide.

Pressurizing modestly to 1.0 MPa (Entry 2) generates quantitative LDC (99%) and enhanced LC (28%) in 48 h, comparing positively to other catalytic systems like CaI_2 78% LDC (5 MPa, with cocatalyst and solvent), Al/Bu_4NCl 85% (1 MPa/66 h), and SILP 79% (5 MPa), while operating metal-free at accessible temperatures, eliminating leaching, separation, and disposal burdens of homogeneous systems. **4-PPIP-H$^+$** thus emerges as a scalable industrial candidate for terpene oxide activation, combining heterogeneous recyclability with green

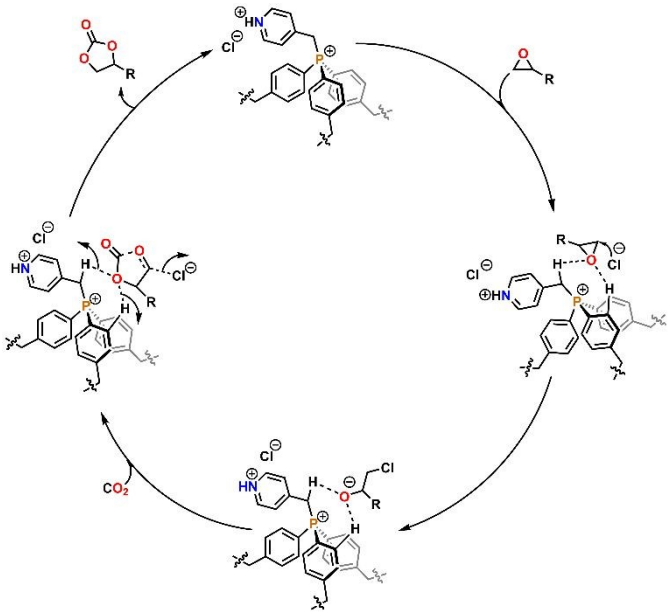

Figure 5: Proposed catalytic pathway for CO_2 cycloaddition through the classical phosphonium-halide route.

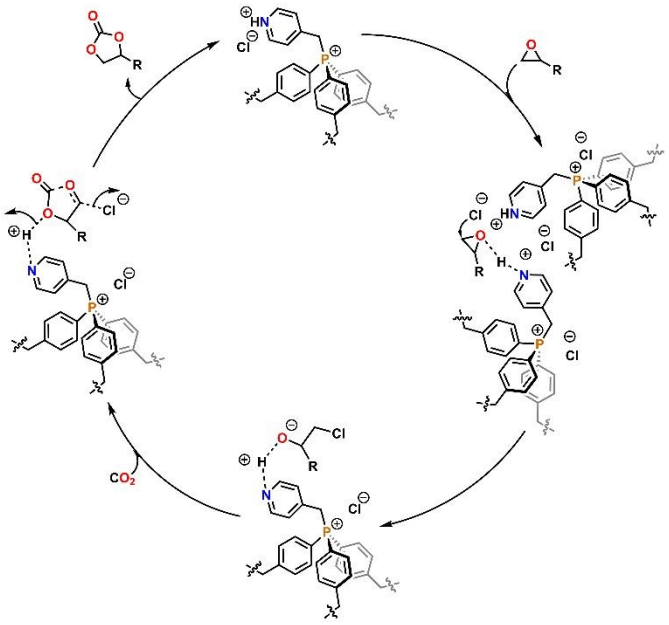

Figure 6: Proposed catalytic pathway for CO_2 cycloaddition through a proton-assisted bifunctional route involving the NH^+ group.

chemistry metrics under accessible pressures without toxic metals.

The catalytic cycle is proposed to proceed through the conventional phosphonium-halide pathway established in our previous work[48], in which chloride initiates epoxide ring opening, followed by CO_2 insertion and cyclization to form the cyclic carbonate. In this mechanism, the phosphonium salt provides the ionic environment, while chloride acts as the nucleophile responsible for the ring-opening step, as shown in **Figure 5**. In the protonated catalyst, the NH^+ group may additionally assist epoxide activation through hydrogen bonding or electrostatic stabilization, which can facilitate the epoxide opening step and strengthen CO_2 insertion, as shown in **Figure 6**. This bifunctional route may therefore explain the higher catalytic activity observed for **4-PPIP-H$^+$**. This proposal is consistent with recent reports from Dai and Xiong groups showing that protonated or hydrogen-bond-donating functional groups can promote epoxide activation and accelerate CO_2 cycloaddition in porous catalytic frameworks.[60-63]

Recyclability

The operational stability of the optimal catalyst **4-PPIP-H$^+$** was evaluated through consecutive recycling experiments using epichlorohydrin (2.5 mmol, 25 mg catalyst, 120 °C, 6 h). After each run, the catalyst was recovered by methanol washing, filtration, and vacuum drying, with yields decreasing from 99% to 88% over four cycles primarily due to minor material losses in catalyst (~2 mg/cycle) during filtration/washing, common for small-scale powder handling. Selectivity remained >99.9% with no byproducts (**Figure 7**). Post-reaction FT-IR analysis (Figure S26) confirmed retention of characteristic phosphonium and pyridinium bands, indicating structural integrity. These results demonstrate excellent chemoselectivity and operational stability of this heterogeneous catalyst.

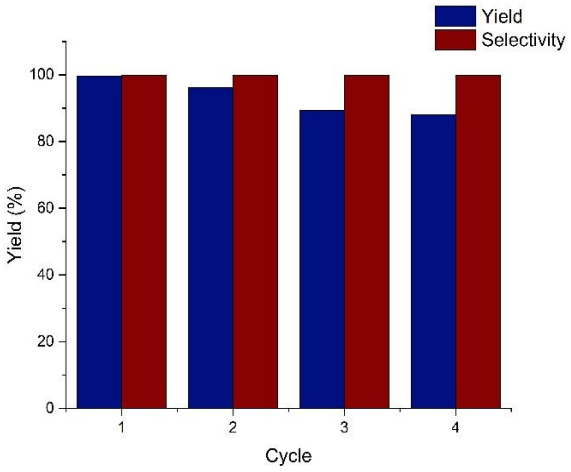

Figure 7. Recyclability of **4-PPIP-H$^+$** over four consecutive runs. Reaction conditions: ECH (2.5 mmol), 25 mg catalyst, 120 °C, 6 h, CO_2 pressure (0.1 MPa).

Conclusions

In summary, we report a series of pyridyl-functionalized porous ionic polymers as efficient, metal-free heterogeneous catalysts for the cycloaddition of CO_2 to epoxides. The *para*-substituted catalyst (**4-PPIP**) demonstrated superior performance over *ortho*- and *meta*-isomers, achieving 90% yield under mild, solvent-free conditions. Protonation of the pyridyl nitrogen significantly enhanced catalytic activity under catalyst-limited conditions (2.3-times rate enhancement) while maintaining structural integrity throughout extended operation, a key advantage over homogeneous analogs that suffer rapid degradation. Remarkably, heterogenization prevented phosphine oxide formation, which was observed in the homogeneous system, enabling stable operation over four consecutive catalytic cycles.

Systematic investigation of synthetic strategies revealed that direct monomer polymerization is essential for maximizing active site density and maintaining optimal pore architecture. Post-functionalization approaches, despite generating higher surface areas, resulted in dramatically reduced activity due to sparse active site loading and pore blockage. Under optimized conditions (120 °C, 6 h, 0.1 MPa CO_2), **4-PPIP-H$^+$** achieved near-quantitative conversion of styrene oxide (98%) and demonstrated broad substrate tolerance across terminal epoxides including sterically hindered bio-based substrates.

These findings establish clear structure-activity relationships for heterogeneous phosphonium catalysts and provide rational design principles for next-generation metal-free CO_2 utilization systems. The combination of high activity, stability, and recyclability positions **PPIP**s as promising candidates for sustainable cyclic carbonate production. This work demonstrates that heterogenized phosphonium catalysts offer a compelling alternative to metal-based and homogeneous systems for CO_2 valorization, combining the low material cost

and metal-free nature of organocatalysts with the robustness, easy separation, and reusability usually associated with heterogeneous MOF or supported metal catalysts. Unlike our earlier reported homogeneous analogs, the polymeric framework confers exceptional durability, enabling catalyst reuse over multiple cycles without loss of activity through phosphine oxide formation. The broad substrate scope, including challenging bio-based terpenes, combined with mild operating conditions (0.1 MPa CO_2, 120 °C, solvent-free) and operational stability establishes **PPIP**s as scalable, cost-effective, and environmentally benign platforms for industrial cyclic carbonate production.

Conflicts of interest

The authors declare no conflict of interest.

Data availability

The data that support the findings of this study are available from the corresponding author upon reasonable request.

Acknowledgements

FGF acknowledges NSERC for a Canada Research Chair and the NSERC CREATE centre CIRCUIT for funding. SK acknowledges CRIBIQ and NSERC for financial support. FGF also acknowledges CCVC (FRQNT).

References

1. H. Hughes, *The IPCC and the politics of writing climate change*, Cambridge University Press, 2024, https://doi.org/10.1017/9781009341554.
2. A. W. Kleij, M. North and A. Urakawa, *ChemSusChem*, 2017, 1-4, https://doi.org/10.1002/cssc.201700218.
3. Q.-W. Song, Z.-H. Zhou and L.-N. He, *Green Chem.*, 2017, **19**, 3707–3728, https://doi.org/10.1039/c7gc00199a.
4. A. Dibenedetto and F. Nocito, *ChemSusChem*, 2020, **13**, 6219–6228, https://doi.org/10.1002/cssc.202002029.
5. M. Aresta, A. Dibenedetto and A. Angelini, *Chem. Rev.*, 2014, **114**, 1709–1742 https://doi.org/10.1021/cr4002758.
6. J. Artz, T. E. Müller, K. Thenert, J. Kleinekorte, R. Meys, A. Sternberg, A. Bardow and W. Leitner, *Chem. Rev.*, 2018, **118**, 434–504, https://doi.org/10.1021/acs.chemrev.7b00435.
7. M. North, R. Pasquale and C. Young, *Green Chem.*, 2010, **12**, 1514–1539, https://doi.org/10.1039/c0gc00065e.
8. R. Turnaturi, C. Zagni, V. Patamia, V. Barbera, G. Floresta and A. Rescifina, *Green Chem.*, 2023, **25**, 9574–9602, https://doi.org/10.1039/d3gc02796a.
9. S. Fukuoka, M. Kawamura, K. Komiya, M. Tojo, H. Hachiya, K. Hasegawa, M. Aminaka, H. Okamoto, I. Fukawa and S. Konno, *Green Chem.*, 2003, **5**, 497–507, https://doi.org/10.1039/b304963a.
10. J. H. Clements, *Ind. Eng. Chem. Res.*, 2003, **42**, 663–674, https://doi.org/10.1021/ie020678i.
11. R. R. Shaikh, S. Pornpraprom and V. D'Elia, *Acs Catal.*, 2018, **8**, 419–450, https://doi.org/10.1021/acscatal.7b03580.
12. H. Büttner, J. Steinbauer, C. Wulf, M. Dindaroglu, H. G. Schmalz and T. Werner, *ChemSusChem*, 2017, **10**, 1076–1079, https://doi.org/10.1002/cssc.201601163.
13. R. Luo, M. Chen, F. Zhou, J. Zhan, Q. Deng, Y. Yu, Y. Zhang, W. Xu and Y. Fang, *J. Mater. Chem. A*, 2021, **9**, 25731–25749, https://doi.org/10.1039/d1ta08146b.
14. M. Liu, X. Wang, Y. Jiang, J. Sun and M. Arai, *Catal. Rev.*, 2019, **61**, 214-269, https://doi.org/10.1080/01614940.2018.1550243.
15. D.-G. Yu and L.-N. He, *Green Chem.*, 2021, **23**, 3499–3501, https://doi.org/10.1039/d1gc90036f.
16. K. Chen, Y. Wu, Z. Zhang, Y. Yang and R. Luo, *Dalton Trans*, 2024, **53**, 2073–2081, https://doi.org/10.1039/d3dt03627h.
17. J. Wang, J. G. W. Yang, G. Yi and Y. Zhang, *Chem. Commun.*, 2015, **51**, 15708–15711, https://doi.org/10.1039/c5cc06295k.
18. S. M. M. Nataj, S. Kaliaguine and F.-G. Fontaine, *Appl. Catal., A*, 2025, **697**, 120186, https://doi.org/10.2139/ssrn.4848203.
19. J. Liang, Y.-B. Huang and R. Cao, *Coord. Chem. Rev.*, 2019, **378**, 32–65, https://doi.org/10.1016/j.ccr.2017.11.013.
20. T. K. Pal, D. De and P. K. Bharadwaj, *Coord. Chem. Rev.*, 2020, **408**, 213173, https://doi.org/10.1016/j.ccr.2019.213173.
21. L. Q. Qiu, H. R. Li and L. N. He, *Acc. Chem. Res.*, 2023, **56**, 2225–2240, https://doi.org/10.1021/acs.accounts.3c00316.
22. S. M. M. Nataj, K. Ouellet, S. Kaliaguine and F. G. Fontaine, *ChemCatChem*, 2024, **17.5**, e202401630, https://doi.org/10.1002/cctc.202401630.
23. S. M. M. Nataj, S. Kaliaguine and F.-G. Fontaine, *Catal. Today*, 2023, **422**, 114216, https://doi.org/10.1016/j.cattod.2023.114216.
24. B.-B. Lu, J. Yang, Y.-Y. Liu and J.-F. Ma, *Inorg. Chem.*, 2017, **56**, 11710–11720, https://doi.org/10.1021/acs.inorgchem.7b01685.
25. Q. Han, L. Wang, Z. Shi, C. Xu, Z. Dong, Z. Mou and W. Liu, *Chem. – Asian J.*, 2017, **12**, 1364–1373, https://doi.org/10.1002/asia.201700418.
26. C. Xu, Y. Liu, L. Wang, J. Ma, L. Yang, F.-X. Pan, A. M. Kirillov and W. Liu, *Dalton Trans*, 2017, **46**, 16426–16431, https://doi.org/10.1039/c7dt03574h.
27. M. Ramin, F. Jutz, J.-D. Grunwaldt and A. Baiker, *J. Mol. Catal. A:Chem.*, 2005, **242**, 32–39, https://doi.org/10.1016/j.molcata.2005.08.004.
28. Q. Zhang, S. Zhang and S. Li, *Macromol.*, 2012, **45**, 2981–2988, https://doi.org/10.1021/ma300278d.
29. K. Hu, Y. Tang, J. Cui, Q. Gong, C. Hu, S. Wang, K. Dong, X. Meng, Q. Sun and F.-S. Xiao, *Chem. Commun.*, 2019, **55**, 9180–9183, https://doi.org/10.1039/c9cc05051e.
30. V. Caló, A. Nacci, A. Monopoli and A. Fanizzi, *Org. lett.*, 2002, **4**, 2561–2563, https://doi.org/10.1002/chin.200248123.
31. Z. Dai, Y. Tang, F. Zhang, Y. Xiong, S. Wang, Q. Sun, L. Wang, X. Meng, L. Zhao and F.-S. Xiao, Chin. *J. Catal.*, 2021, **42**, 618–626, https://doi.org/10.1016/s1872-2067(20)63679-8.

32. *Industrial Green Chemistry*, ed. S. Kaliaguine and J.-L. Dubois, Walter de Gruyter GmbH & Co KG, 2nd edn, 2025, https://doi.org/10.1515/9783110646856.
33. S. Zhong, L. Tian, L. Yi, Y. Liu, W. Cheng, Y. Wang and Y. Li, *J. Environ. Chem. Eng.*, 2023, **11**, 109883, https://doi.org/10.1016/j.jece.2023.109883.
34. R. Luo, Y. Yang, K. Chen, X. Liu, M. Chen, W. Xu, B. Liu, H. Ji and Y. Fang, *J. Mater. Chem. A*, 2021, **9**, 20941–20956, https://doi.org/10.1039/d1ta05428g.
35. A. Morena, V. Campisciano, A. Santiago-Portillo, M. Gruttadauria, F. Giacalone and C. Aprile, *Fuel*, 2023, **336**, 126819, https://doi.org/10.1016/j.fuel.2022.126819.
36. V. Campisciano, L. Valentino, A. Morena, A. Santiago-Portillo, N. Saladino, M. Gruttadauria, C. Aprile and F. Giacalone, *J. CO2 Util.*, 2022, **57**, 101884, https://doi.org/10.1016/j.jcou.2022.101884.
37. K. Su, W. Wang, B. Li and D. Yuan, *ACS Sustainable Chem. Eng.*, 2018, **6**, 17402–17409, https://doi.org/10.1021/acssuschemeng.8b05203.
38. Z. Dai, S. Wang, N. Zhou, Y. Liu and Y. Xiong, *New J. Chem.*, 2022, **46**, 22151–22161, https://doi.org/10.1039/d2nj04210j.
39. S. Jayakumar, H. Li, L. Tao, C. Li, L. Liu, J. Chen and Q. Yang, *ACS Sustainable Chem. Eng.*, 2018, **6**, 9237–9245, https://doi.org/10.1021/acssuschemeng.8b01548.
40. R. Luo, X. Liu, M. Chen, B. Liu and Y. Fang, *ChemSusChem*, 2020, **13**, 3945–3966, https://doi.org/10.1002/cssc.202001079.
41. Z. Dai, Q. Sun, X. Liu, C. Bian, Q. Wu, S. Pan, L. Wang, X. Meng, F. Deng and F.-S. Xiao, *J. Catal.*, 2016, **338**, 202–209, https://doi.org/10.1016/j.jcat.2016.03.005.
42. L. Valentino, C. Célis, V. Campisciano, M. Gruttadauria, C. Aprile and F. Giacalone, *ChemCatChem*, 2024, **16**, e202301428, https://doi.org/10.1002/cctc.202301428.
43. E. Yasar, E. Aytar and A. Kilic, *Inorganica Chimica Acta*, 2025, **577**, 122503, https://doi.org/10.1016/j.ica.2024.122503.
44. A. Kilic, E. Yasar and E. Aytar, *Sustainable Energy & Fuels*, 2019, **3**, 1066-1077, https://doi.org/10.1039/c8se00633d.
45. A. Tumbul, E. Yasar and A. Kilic, *Reaction Chemistry & Engineering*, 2026, https://doi.org/10.1039/d5re00369e.
46. A. Kilic, E. Yasar, H. I. b. Önal, F. Koyuncu, M. Aydemir and F. Durap, *Energy & Fuels*, 2025, **39**, 23241-23258, https://doi.org/10.1039/c8se00633d.
47. X. Liu, Y. Yang, M. Chen, W. Xu, K. Chen and R. Luo, *ACS Appl. Mater. Interfaces*, 2022, **15**, 1085–1096, https://doi.org/10.1021/acsami.2c18283.
48. A. Enferadikerenkan, M. Beillard, G. Wang, T. Rajeshkhumar, L. Maron, S. Kaliaguine and F. G. Fontaine, *ChemCatChem*, 2026, **18**, e01396, https://doi.org/10.1002/cctc.202501396.
49. Q. Sun, M. Jiang, Z. Shen, Y. Jin, S. Pan, L. Wang, X. Meng, W. Chen, Y. Ding and J. Li, *Chem. Commun.*, 2014, **50**, 11844–11847, https://doi.org/10.1039/c4cc03884c.
50. F. K. Metze, S. Sant, Z. Meng, H. A. Klok and K. Kaur, *Langmuir*, 2023, **39**, 3546–3557, https://doi.org/10.1021/acs.langmuir.2c02801.
51. M. Chen, B. Coasne, R. Guyer, D. Derome and J. Carmeliet, *Nat. commun.*, 2018, **9**, 3507, https://doi.org/10.1038/s41467-018-05897-9.
52. F. Della Monica and A. W. Kleij, *Polym. Chem.*, 2020, **11**, 5109–5127, https://doi.org/10.1039/d0py00817f.
53. A. Belinchon, E. Hernandez, J. Vazquez, R. Santiago, C. Moya, M. Larriba, P. Navarro and J. Palomar, *ACS Sustainable Chem. Eng.*, 2022, **10**, 9635–9643, https://doi.org/10.1021/acssuschemeng.2c02993.
54. P. Miksovsky, E. N. Horn, S. Naghdi, D. Eder, M. Schnürch and K. Bica-Schröder, *Org. Process Res. Dev.*, 2022, **26**, 2799–2810, https://doi.org/10.1021/acs.oprd.2c00143.
55. V. Aomchad, À. Cristòfol, F. Della Monica, B. Limburg, V. D'Elia and A. W. Kleij, *Green Chem.*, 2021, **23**, 1077–1113, https://doi.org/10.1039/d0gc03824e.
56. N. Bragato, A. Perosa, M. Selva, G. Fiorani and R. Calmanti, *Green Chem.*, 2023, **25**, 4849–4860, https://doi.org/10.1039/d2gc04475g.
57. M. Navarro, A. Garces, L. F. Sanchez-Barba, D. Gonzalez-Lizana and A. Lara-Sanchez, *Dalton Trans*, 2023, **52**, 6105–6116, https://doi.org/10.1039/d3dt00510k.
58. L. Longwitz, J. Steinbauer, A. Spannenberg and T. Werner, *ACS Catal.*, 2018, **8**, 665–672, https://doi.org/10.1021/acscatal.7b03367.
59. F. de la Cruz-Martínez, M. Martínez de Sarasa Buchaca, J. Martínez, J. Fernández-Baeza, L. F. Sánchez-Barba, A. Rodríguez-Diéguez, J. A. Castro-Osma and A. Lara-Sánchez, *ACS Sustainable Chem. Eng.*, 2019, **7**, 20126–20138, https://doi.org/10.1021/acssuschemeng.9b06016.
60. W. Ma, N. Zhou, Y. Wu, L. Qiu, C. Jin, F. Xue, Z. Dai and Y. Xiong, *Fuel*, 2026, **421**, 139090, https://doi.org/10.1016/j.fuel.2026.139090.
61. T. Peng, N. Zhou, C. Zhang, X. Yang, X. Meng, Z. Dai and Y. Xiong, *ACS Appl. Mater. Interfaces*, 2024, **16**, 66032-66043, https://doi.org/10.1021/acsami.4c12955.
62. X. Yang, N. Zhou, X. Xie, T. Peng, C. Zhang, X. Meng, Z. Dai and Y. Xiong, *Fuel*, 2025, **389**, 134617, https://doi.org/10.1016/j.fuel.2025.134617.
63. C. Zhang, N. Zhou, S. Wang, X. Yang, T. Peng, Z. Dai, F. Xiang and Y. Xiong, *J. CO2 Utili*, 2024, **88**, 102954, https://doi.org/10.1016/j.jcou.2024.102954.

View Article Online
DOI: 10.1039/D6MA00580B

The data supporting this article have been included as part of the Supplementary Information.